# Guidelines for choosing molecular "alligator clip" binding motifs in electron transport devices

Matthew G. Reuter,[a] Tamar Seideman, and Mark A. Ratner
*Department of Chemistry, Northwestern University, Evanston, Illinois 60208-3113, USA*

(Received 4 February 2011; accepted 1 April 2011; published online 21 April 2011)

We employ a one-electron, tight-binding model of an electrode–molecule–electrode junction to explore the fundamental relationship between adsorption geometry and electron transport, producing exact results (within this model). By varying the chemisorption location (e.g., atop a surface atom or in a hollow site between surface atoms) and the molecule–electrode coupling, we find that the largest currents are realized when the molecule (i) is highly coordinated by the surface and (ii) has favorable overlap with electrode states near the Fermi level. We also show the importance of electrode-induced molecular level shifting for certain adsorption geometries, which can cause molecular levels far from the Fermi level to conduct better than those near the Fermi level. Since all of these factors are greatly influenced by the chemical moiety used to link the molecule to an electrode, these results present a set of guidelines to help choose "alligator clips" for molecular electronic devices. © *2011 American Institute of Physics*. [doi:10.1063/1.3581097]

The idea of using molecules as components in electrical circuits—molecular electronics[1]—is appealing for its conceptual content and technological applications. The wide synthetic variability and nanometer-scale sizes of molecular systems offer the potential to build smaller, faster, and more efficient electrical devices. Understanding how electric current flows through molecular wires is crucial to realizing these technologies, and has challenged both experimental and theoretical studies.[2,3] Experiments require novel techniques and approaches to construct and characterize such systems, and theoretical efforts must combine electronic structure, chemisorption, nonequilibrium approaches, and scattering theories.

Previous research has illuminated two key details for describing electron transport: (i) the electronic structure of the molecular wire[4–13] and (ii) the interface(s) between the molecular wire and the electrode(s).[3,5,11,13–28] Investigations into the former have identified the conceptual importance of the wires' molecular orbitals (MOs); in a one-electron picture, the MOs must provide pathways for electrons through the molecular wire.[4,6] Moreover, the phase relations and symmetries of the MOs can lead to quantum interference effects[7] and selection rules guiding where to connect the molecule to the electrodes.[5,7,8,10,12] Using these results, knowledge of a candidate wire's MOs helps predict the wire's electron transport properties; that is, the MO structure provides chemical intuition for designing molecular wires.

Studies of the interface, on the other hand, build on chemisorption theory and aim to devise molecular "alligator clips" to link molecular wires and electrodes. The adsorption geometry[14,15,17,19,26–28] and the strength of coupling between the wire and the electrode[5,23,25,26] are important considerations; chemisorption broadens and shifts the wire's MOs. In essence, we seek alligator clips that robustly link the components without impeding current. The gold–thiol combination has been particularly well-studied as an alligator clip,[15,18,24–26,29] finding that thiols bind to gold in many configurations.[29] For example, the thiol can perch atop an individual gold atom or nestle in a threefold hollow site between gold atoms. Other linking moieties, including amines and isothiocyanides, have also been investigated and display a myriad of adsorption chemistries on various metals (e.g., platinum and silver).[11,13,17,18,20,21,26,30] With these many choices for alligator clips, the question remains, "What fundamental characteristics are desirable for anchoring molecular wires to electrodes?" Unlike the case for the wire's MOs, our chemical intuition is insufficient to predict electron transport properties from knowledge of how a linking moiety chemisorbs to a metallic electrode.

In this paper we explore the relationship between adsorption chemistry and electron transport through molecular wires. By employing a phenomenological, tight-binding model, we are able to abstract the fundamental role of chemisorption in electron transport. Moreover, all of our results are analytical and exact (within the model). After introducing our model, we calculate electron transport through various electrode-molecular wire–electrode systems within the Landauer–Imry (coherent scattering) formalism.[31] Finally, we discuss these results, developing several guidelines for choosing molecular alligator clips.

Our model represents the molecular wire by a single level, $|\varphi\rangle$, with energy $\alpha$, i.e., $\langle\varphi|\mathcal{H}_{\text{mol}}|\varphi\rangle = \alpha$, where $\mathcal{H}_{\text{mol}}$ is the molecular wire's Hamiltonian. This level is conceivably the wire's highest-occupied or lowest-unoccupied MO. Likewise, each electrode is composed of identical single-state sites arranged in a semi-infinite cubic lattice, where each site's state has energy $\varepsilon$ and only couples to its nearest neighbors with element $V_e$. Such an electrode represents a generic, single-band metal, and exhibits a band of width $12|V_e|$ centered around $\varepsilon$.[22,32–34] Finally, we define $\varepsilon = 0$

[a]Electronic mail: mgreuter@u.northwestern.edu.

 © 2011 American Institute of Physics

Downloaded 29 Jul 2011 to 129.105.55.246. Redistribution subject to AIP license or copyright; see http://jcp.aip.org/about/rights_and_permissions

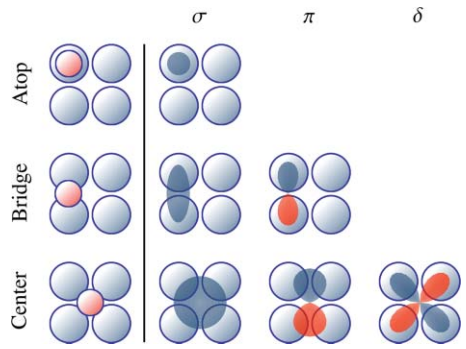


FIG. 1. Chemisorption geometries and overlaps considered throughout this work. The "atop" binding configuration (top row) places the molecule (small, red circle) atop a single electrode site (larger blue circle). The "bridge" (middle row) and "center" (bottom row) configurations nestle the molecule between two and four electrode sites, respectively. The MO symmetry effects the nature of electrode–molecule coupling, causing the molecule to interact differently with the various electrode sites. For our purposes, a $\sigma$ MO has no nodal planes perpendicular to the surface, whereas $\pi$ and $\delta$ MOs have one and two such nodal planes, respectively. These symmetries are drawn in the rightmost columns, where "constructive" and "destructive" molecule–electrode overlaps are depicted in blue and red, respectively.

eV (for convenience) and denote the states at the electrode's surface by $|m, n\rangle$, where $m$ and $n$ are integers.

Having described our molecular wire and electrodes independently, we now need to couple them together. For the moment, we only discuss chemisorption of the wire to a single electrode; the other electrode is treated similarly. The simplest coupling occurs when the wire sits atop a single electrode site, as depicted in the top-left corner of Fig. 1. In this case, the wire–electrode coupling operator, $\mathcal{V}$, is

$$\mathcal{V}_{\text{atop}} = V_{0,0}\,|\varphi\rangle\,\langle 0,0\,|. \tag{1a}$$

We also consider two other adsorption schemes, the bridge and center configurations, as shown in the middle and bottom rows of Fig. 1, respectively.[33,35] In the bridge configuration, the wire sits in between two surface sites such that

$$\mathcal{V}_{\text{bridge}} = V_{0,0}\,|\varphi\rangle\,\langle 0,0| + V_{0,1}\,|\varphi\rangle\,\langle 0,1|\,, \tag{1b}$$

whereas the center geometry nestles the wire in the hollow site among four surface sites,

$$\begin{aligned}\mathcal{V}_{\text{center}} = {} & V_{0,0}\,|\varphi\rangle\,\langle 0,0| + V_{0,1}\,|\varphi\rangle\,\langle 0,1| + V_{1,0}\,|\varphi\rangle\,\langle 1,0| \\ & + V_{1,1}\,|\varphi\rangle\,\langle 1,1|\,.\end{aligned} \tag{1c}$$

For simplicity, we assume the wire couples to each electrode site with uniform strength, that is, $|V_{m,n}| = V$. In these cases, we can still choose the sign of each $V_{m,n}$, which relates to the overlap between the electrode and the wire.[5] This point is best described illustratively. Suppose that each electrode site contributes an $s$-like orbital,[32,33] as gold may,[11] and that the wire is chemisorbed in the center configuration. If the wire's MO has $\sigma$ symmetry (i.e., no nodal planes) perpendicular to the surface, the MO will constructively (or destructively) overlap with all four electrode states. Similarly, a $\pi$ MO (one nodal plane) will constructively overlap with two adjacent electrode states and destructively overlap with the other two. Lastly, a $\delta$ MO (two nodal planes) will constructively overlap with two kitty-cornered states and destructively overlap with the others. These three scenarios are diagrammed in Fig. 1, along with the likewise scenarios for the atop and bridge configurations.

TABLE I. Parameters for the six electrode–molecular wire coupling schemes displayed in Fig. 1.

| | $\mathcal{V}^{\sigma}_{\text{atop}}$ | $\mathcal{V}^{\sigma}_{\text{bridge}}$ | $\mathcal{V}^{\pi}_{\text{bridge}}$ | $\mathcal{V}^{\sigma}_{\text{center}}$ | $\mathcal{V}^{\pi}_{\text{center}}$ | $\mathcal{V}^{\delta}_{\text{center}}$ |
|---|---|---|---|---|---|---|
| $V_{0,0}$ | $-V$ | $-V$ | $-V$ | $-V$ | $-V$ | $-V$ |
| $V_{0,1}$ | 0 | $-V$ | $V$ | $-V$ | $-V$ | $V$ |
| $V_{1,0}$ | 0 | 0 | 0 | $-V$ | $V$ | $V$ |
| $V_{1,1}$ | 0 | 0 | 0 | $-V$ | $V$ | $-V$ |

While more complicated circumstances for these orbital overlap situations are possible,[35,36] they do not alter the fundamental picture; the wire's terminal state will still either constructively or destructively overlap with the particular electrode states. Using the convention that $V_{m,n} < 0$ for constructive overlap ($V_{m,n} > 0$ is destructive), the six wire–electrode coupling schemes we consider here are listed in Table I.

We assemble the total system by sandwiching the wire between two electrodes, and, for simplicity, assume the wire couples to both electrodes in the same manner. Due to our focused interest in electron transport through the molecular wire and the vast (infinite) sizes of the electrodes, we write an effective Hamiltonian for the wire,

$$\mathcal{H} \to \mathcal{H}_{\text{mol}} + 2\Sigma(E), \tag{2}$$

where $\Sigma(E)$ is the self-energy of coupling the wire to one electrode,[37] and the factor of 2 reflects identical coupling to both electrodes. In essence, this self-energy changes the boundary conditions for the isolated wire to account for interactions with an electrode, which is no longer explicitly considered. The real part[38] of $\Sigma(E)$ describes how the molecular level is shifted upon chemisorption, whereas the imaginary part of $\Sigma(E)$ pertains to the broadening of the level. Formally,[37]

$$\Sigma(E) = \mathcal{V}\mathcal{G}_{\text{elec}}(E)\mathcal{V}^{\dagger}, \tag{3}$$

where $\mathcal{G}_{\text{elec}}(E)$ is the (retarded) Green function of the isolated electrode. For the electrodes used here, $\mathcal{G}_{\text{elec}}(E)$ has semianalytical matrix elements,[34]

$$\begin{aligned}\mathbf{G}_{|m-m'|,|n-n'|}(E) &\equiv \left\langle m', n'\,|\mathcal{G}_{\text{elec}}(E)|\,m, n\right\rangle \\ &= \frac{1}{|V_e|\pi^2}\int_0^{\pi} \mathrm{d}\theta_1 \cos(|m-m'|\theta_1)\int_0^{\pi}\mathrm{d}\theta_2 \\ &\quad \times \cos(|n-n'|\theta_2)\Xi[E/(2|V_e|) + \cos(\theta_1) \\ &\quad + \cos(\theta_2)],\end{aligned} \tag{4}$$

where

$$\Xi(x) = x + [\Theta(-x-1) - \Theta(x+1)]\sqrt{x^2-1}, \tag{5}$$

$V_e$ is the electrode's nearest-neighbor coupling, and $\Theta(x)$ is the Heaviside step function. Note that $\mathcal{G}_{\text{elec}}(E)$ is symmetric, that is, $\mathbf{G}_{m,n}(E) = \mathbf{G}_{n,m}(E)$.

Downloaded 29 Jul 2011 to 129.105.55.246. Redistribution subject to AIP license or copyright; see http://jcp.aip.org/about/rights_and_permissions

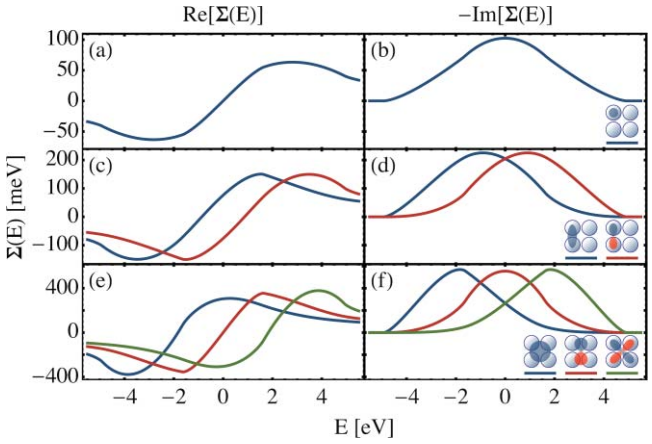


FIG. 2. Self-energies for the six chemisorption geometries pictured in Fig. 1. The atop/$\sigma$ geometry (top row) exhibits strong molecular level shifting nearer to the band edges (a), with pronounced level broadening at the center of the band (b). A similar situation is observed for the center/$\pi$ geometry [red lines in (e) and (f)]. Conversely, both bridge geometries show level shifting throughout much of the band (c) and level broadening (d) closer to either the bottom (bridge/$\sigma$) or top (bridge/$\pi$) of the band. The center/$\sigma$ and center/$\delta$ geometries parallel the bridge/$\sigma$ and bridge/$\pi$ geometries, respectively.

The synthesis of Eqs. (1), (3), and (4) provides the self-energy for each of the six chemisorption geometries,

$$\Sigma(E) = |V|^2 \left[c_{0,0}\mathbf{G}_{0,0}(E) + c_{0,1}\mathbf{G}_{0,1}(E) + c_{1,1}\mathbf{G}_{1,1}(E)\right], \tag{6}$$

where the expansion coefficients are listed in Table II. Following Sec. 5 of Ref. 22, we choose model parameters to be representative of realistic systems, $V = 0.4$ eV and $V_e = -0.82$ eV, and plot the six self-energies in Fig. 2. The atop/$\sigma$ and center/$\pi$ geometries display more level shifting toward the band edges than in the center, but more level broadening in the band center. Besides subtle differences in the lineshapes of $\Sigma^{\sigma}_{\text{atop}}(E)$ and $\Sigma^{\pi}_{\text{center}}(E)$, the biggest disparity is the change in their magnitude; $\Sigma^{\pi}_{\text{center}}(E) \approx 5\Sigma^{\sigma}_{\text{atop}}(E)$. This stems from two sources. First, comparison of the expansion coefficients in Table II shows an inherent factor of 4. Second, we use the same $|V|$ for both cases to facilitate a direct comparison of the various geometries. $|V|$ is probably dependent on the specific geometry, and reducing $|V|$ for the center/$\pi$ case mitigates this disparity.

The other four bonding geometries are less symmetric about the band center. For example, the bridge/$\sigma$ geometry displays moderate level shifting throughout the band, and the broadening peaks below the band center. The most apparent trend is in the imaginary parts, where the $\sigma$ geometries peak at lower energies than the $\pi$ geometries, and so forth for the $\delta$ geometries. Imagining the electrode eigenstates as classical waves,[33,36] electrode states with fewer nodes, which appear at the bottom of the band, will exhibit better overlap with the $\sigma$ MOs. Similarly, electrode states with more nodes will have higher energies and interact more strongly with the $\pi$ and $\delta$ MOs. Lastly, Table II and Fig. 2 show symmetry between $\Sigma^{\sigma}_{\text{bridge}}(E)$ and $\Sigma^{\pi}_{\text{bridge}}(E)$, and likewise between $\Sigma^{\sigma}_{\text{center}}(E)$ and $\Sigma^{\delta}_{\text{center}}(E)$. Specifically, the imaginary parts are mirror images of each other, while the real parts are mirror images with a sign inversion.

TABLE II. Each chemisorption geometry's set of self-energy expansion coefficients for use in Eq. (6).

| | $\Sigma^{\sigma}_{\text{atop}}$ | $\Sigma^{\sigma}_{\text{bridge}}$ | $\Sigma^{\pi}_{\text{bridge}}$ | $\Sigma^{\sigma}_{\text{center}}$ | $\Sigma^{\pi}_{\text{center}}$ | $\Sigma^{\delta}_{\text{center}}$ |
|---|---|---|---|---|---|---|
| $c_{0,0}$ | 1 | 2 | 2 | 4 | 4 | 4 |
| $c_{0,1}$ | 0 | 2 | −2 | 8 | 0 | −8 |
| $c_{1,1}$ | 0 | 0 | 0 | 4 | −4 | 4 |

Mindful of these varying adsorption chemistries, we proceed to examine their effects on electron transport. At zero temperature and within a coherent scattering formalism,[31] the current through the molecular wire (assuming equivalent coupling to both electrodes) is

$$I(V) = \frac{2e}{h}\int_{E_F - eV/2}^{E_F + eV/2} \mathrm{d}E\, T(E), \tag{7}$$

where $I$ is the current, $V$ is the applied bias voltage, $E_F$ is the Fermi level, $e$ is the electron charge, $h$ is Planck's constant, and $T(E)$ is the transmission, that is, the probability that an electron at energy $E$ successfully transmits from one electrode to the other through the wire. For the systems considered here, the transmission is[31]

$$T(E) = \frac{4\,(\mathrm{Im}\Sigma(E))^2}{|E - \alpha - 2\Sigma(E)|^2}. \tag{8}$$

Finally, the calculations that follow take $E_F = 0$ eV, although we discuss the ramifications of alternate choices.

We begin with the electron transport of wires bound in the center configuration. The solid lines in Fig. 3 depict the transmission and corresponding current/voltage spectra for these geometries. Examining the center/$\sigma$ (and, symmetrically, center/$\delta$) geometry, we see a broad transmission peak for a molecular level in the bottom of the band (blue line).

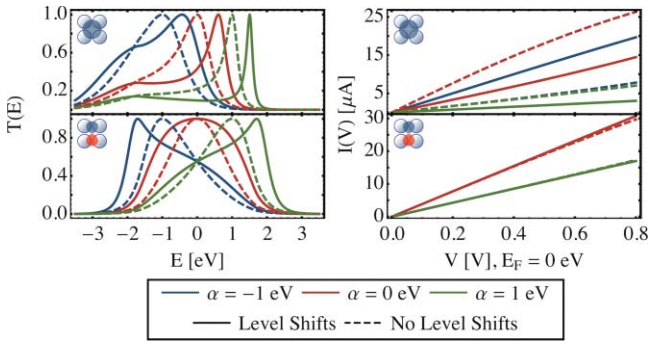


FIG. 3. The transmission (left column) and current/voltage (right column) spectra for molecular wires bound in the center configuration. The top row displays the center/$\sigma$ geometry, while the bottom row is the center/$\pi$ geometry. Due to its symmetry with the center/$\sigma$ geometry, we omit the center/$\delta$ geometry. In all cases, the blue lines correspond to a molecular level with $\alpha = -1$ eV, the red lines $\alpha = 0$ eV, and the green lines $\alpha = 1$ eV. The exact spectra (pictured in solid lines) show that the MO overlap structure is important; there is a roughly twofold change in current between the two geometries for all wires. Moreover, the maximum current is realized for the $\alpha = -1$ eV wire in the center/$\sigma$ geometry, despite $E_F = 0$ eV. Finally, neglecting the level shifting (dashed lines) is ill-advised, particularly for the center/$\sigma$ geometry, since it can produce twofold differences in currents through the wires. Note that some of the blue and green lines overlap in the current/voltage spectra.

Downloaded 29 Jul 2011 to 129.105.55.246. Redistribution subject to AIP license or copyright; see http://jcp.aip.org/about/rights_and_permissions

The molecular levels in the center (red) and top (green) of the band have reduced, but nonzero, transmission over most of the band. Turning to the current, the molecular level at the top of the band is off resonance, displaying little current, whereas the other two levels both yield moderate currents. Surprisingly, the molecular level at the bottom of the band exhibits higher current than the level in the center, which is at the Fermi level.

Molecular level shifting, as described by the real part of $\Sigma(E)$, is responsible for this unintuitive result. From the locations of the transmission peaks, adsorbing in the center/$\sigma$ geometry shifts these molecular levels toward the upper band edge [Fig. 2(a)] such that the molecular level with $\alpha = 0$ eV moves off resonance. While the $\alpha = -1$ eV molecular level is not sufficiently shifted to be resonant at $E_F$, the level's broadening [Fig. 2(b)] produces large transmissions around $E_F$.

To further demonstrate the culpability of level shifting for these observations, the dashed lines in Fig. 3 show the transmission and current/voltage spectra in the absence of level shifting.[39] In these cases, the molecular level at the band center remains resonant, and, as expected, displays the largest current. Moreover, the currents for all three levels change twofold without level shifting. Clearly, molecular level shifting is significant for understanding electron transport through wires with the center/$\sigma$ and center/$\delta$ geometries. As a computational aside, the importance of molecular level shifting here may invalidate the wide-band limit when studying electron transport in more sophisticated systems; one of its consequences is a neglect of level shifting.

The center/$\pi$ geometry, also displayed in Fig. 3, exhibits the expected electron transport characteristics: the molecular level in the center of the band (nearest to $E_F$) produces the largest current. The most noteworthy feature here is the large current for this molecular level. This level's broad transmission peak produces a current roughly twice that observed for the same level chemisorbed in the center/$\sigma$ geometry. Furthermore, molecular level shifting is relatively benign, although this is a consequence of our choice of Fermi level (0 eV). Since $\mathrm{Re}\Sigma^{\pi}_{\mathrm{center}}(0\ \mathrm{eV}) = 0$ eV, it is unsurprising that the transmission spectra with and without level shifting all converge at 0 eV. Had we instead chosen $E_F = -1$ eV, molecular level shifting would cause the molecular level in the center of the band to display a larger current than that at $-1$ eV. This parallels the unintuitive observations for the center/$\sigma$ geometries.

Turning to the atop configuration, Fig. 4 displays the transmission and $I/V$ spectra for the atop/$\sigma$ geometry. These spectra are simpler than those for the center geometries; the molecular level closest to the Fermi level generates the largest current and molecular shifting is virtually nonexistent. Finally, the bridge/$\sigma$ (and, symmetrically, bridge/$\pi$) geometry acts as an intermediate between the atop and center geometries. As shown in Fig. 5, the largest current is still realized for the molecular level with $\alpha \approx E_F$ since molecular level shifting, while present, is small.

Recognizing the critical importance of the molecular linking group on adsorption chemistry, these electron transport results elucidate several guidelines for choosing molecular alligator clips. First, current tends to increase with the coordination of the linker. Comparing Figs. 3–5, the

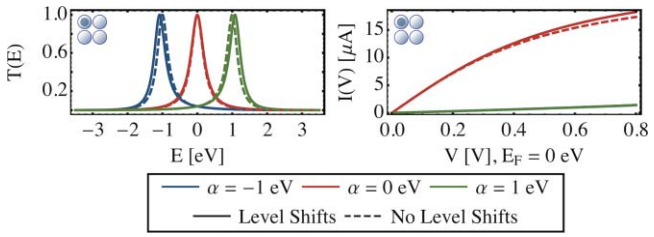


FIG. 4. The transmission and current/voltage spectra for molecular wires bound in the atop configuration. As expected, the molecular level nearest the Fermi level exhibits the largest current. Unlike for the center geometries in Fig. 3, molecular level shifting is less consequential; its neglect barely changes the results.

maximum current of the center geometries is larger than that of the bridge and, likewise, atop geometries. Moreover, this effect is consistent with recent experimental observations.[28] Second, the wire's MO should strongly overlap with the electrode eigenstates near $E_F$. For example, the center/$\pi$ geometry showed the largest current of the three center geometries when the Fermi level was in the middle of the band. If, conversely, the Fermi level were nearer to the bottom of the band, a linker with more $\sigma$ character would likely be preferable, as seen from the transmission spectra in Fig. 3. Finally, the molecular level needs to be at a suitable energy, which due to molecular level shifting, may not be near the Fermi level. This guideline is probably the most obvious and most important, since it encapsulates an intrinsic goal of molecular electronics.

In summary, we used a tight-binding model of an electrode–molecular wire–electrode junction to study the fundamental relationship between chemisorption geometry and electron transport. Our results are exact within this model. We found that the location of the wire on the electrode surface (considered here to be the atop, bridge, or center configuration) and the symmetry of the wire's MO are critical factors. In general, larger currents are realized for (i) chemisorption locations offering more coordination and (ii) MOs strongly overlapping with the electrode eigenstates near the Fermi level. These observations suggest a chemical intuition for correlating chemisorption and electron transport, and also identify important considerations when linking molecular wires to electrodes. Carefully tuning the molecular wire's adsorption

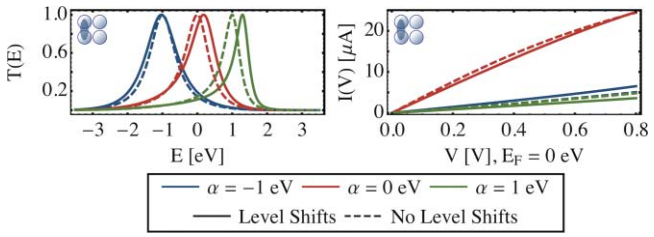


FIG. 5. The transmission and current/voltage spectra for molecular wires bound in the bridge configuration. We omit the bridge/$\pi$ geometry due to its symmetry to the bridge/$\sigma$ geometry. Similar to the atop geometry (Fig. 4), the molecular level nearest to the Fermi level produces the largest current. Molecular level shifting is more noticeable than in the atop geometry, but considerably less significant than in the center geometries (Fig. 3).

Downloaded 29 Jul 2011 to 129.105.55.246. Redistribution subject to AIP license or copyright; see http://jcp.aip.org/about/rights_and_permissions

chemistry, through the judicious choice of molecular alligator clips, has the potential to enhance electron transport.

## ACKNOWLEDGMENTS

We are grateful to Gemma C. Solomon and Shane M. Parker for helpful suggestions. M.G.R. thanks the (U.S.) Department of Energy (DOE) Computational Science Graduate Fellowship Program (Grant No. DE-FG02-97ER25308) for a graduate fellowship. This work was partially supported by the (U.S.) National Science Foundation (NSF) (Grant Nos. CHE-1012207 and CHE-0719420), the MRSEC program of the National Science Foundation (NSF) (DMR-0520513), and the Nonequilibrium Energy Research Center (NERC), which is an Energy Frontier Research Center funded by the (U.S.) Department of Energy (DOE), Office of Science, Office of Basic Energy Sciences under Award No. DE-SC0000989.

[1] A. Aviram and M. A. Ratner, Chem. Phys. Lett. **29**, 277 (1974).
[2] X.-Y. Zhu, Surf. Sci. Rep. **56**, 1 (2004).
[3] S. M. Lindsay and M. A. Ratner, Adv. Mater. **19**, 23 (2007).
[4] M. Magoga and C. Joachim, Phys. Rev. B **56**, 4722 (1997).
[5] C.-C. Kaun, R. Jorn, and T. Seideman, Phys. Rev. B **74**, 045415 (2006).
[6] R. Li, S. Hou, J. Zhang, Z. Qian, Z. Shen, and X. Zhao, J. Chem. Phys. **125**, 194113 (2006).
[7] G. C. Solomon, D. Q. Andrews, T. Hansen, R. H. Goldsmith, M. R. Wasielewski, R. P. Van Duyne, and M. A. Ratner, J. Chem. Phys. **129**, 054701 (2008).
[8] K. Yoshizawa, T. Tada, and A. Staykov, J. Am. Chem. Soc. **130**, 9406 (2008).
[9] G. C. Solomon, D. Q. Andrews, R. P. Van Duyne, and M. A. Ratner, Chem. Phys. Chem. **10**, 257 (2009).
[10] P. W. Fowler, B. T. Pickup, T. Z. Todorova, and W. Myrvold, J. Chem. Phys. **131**, 044104 (2009).
[11] C.-H. Ko, M.-J. Huang, M.-D. Fu, and C.-H. Chen, J. Am. Chem. Soc. **132**, 756 (2010).
[12] X. Li, A. Staykov, and K. Yoshizawa, J. Phys. Chem. C **114**, 9997 (2010).
[13] M. C. Lennartz, V. Caciuc, N. Atodiresei, S. Karthäuser, and S. Blügel, Phys. Rev. Lett. **105**, 066801 (2010).
[14] S. N. Yaliraki and M. A. Ratner, J. Chem. Phys. **109**, 5036 (1998).
[15] E. G. Emberly and G. Kirczenow, Phys. Rev. B **58**, 10911 (1998).
[16] K. W. Hipps, Science **294**, 536 (2001).
[17] J. M. Seminario, C. E. de la Cruz, and P. A. Derosa, J. Am. Chem. Soc. **123**, 5616 (2001).
[18] S.-H. Ke, H. U. Baranger, and W. Yang, J. Am. Chem. Soc. **126**, 15897 (2004).
[19] G. C. Solomon, J. R. Reimers, and N. S. Hush, J. Chem. Phys. **122**, 224502 (2005).
[20] G. Heimel, L. Romaner, E. Zojer, and J.-L. Brédas, Nano Lett. **7**, 932 (2007).
[21] Y. S. Park, A. C. Whalley, M. Kamenetska, M. L. Steigerwald, M. S. Hybertsen, C. Nuckolls, and L. Venkataraman, J. Am. Chem. Soc. **129**, 15768 (2007).
[22] A. Landau, L. Kronik, and A. Nitzan, J. Comput. Theor. Nanosci. **5**, 535 (2008).
[23] Y. F. Wang, J. Kröger, R. Berndt, H. Vázquez, M. Brandbyge, and M. Paulsson, Phys. Rev. Lett. **104**, 176802 (2010).
[24] M. Strange, O. Lopez-Acevedo, and H. Häkkinen, J. Phys. Chem. Lett. **1**, 1528 (2010).
[25] H. Kondo, J. Nara, and T. Ohno, Phys. Rev. B **81**, 085318 (2010).
[26] J. Zhou, G. Chen, and B. Xu, J. Phys. Chem. C **114**, 8587 (2010).
[27] F. Mohn, J. Repp, L. Gross, G. Meyer, M. S. Dyer, and M. Persson, Phys. Rev. Lett. **105**, 266102 (2010).
[28] G. Schull, T. Frederiksen, A. Arnau, D. Sánchez-Portal, and R. Berndt, Nature Nanotechnol. **6**, 23 (2011).
[29] A. Bilić, J. R. Reimers, and N. S. Hush, J. Chem. Phys. **122**, 094708 (2005).
[30] E. de la Llave, A. Ricci, E. J. Calvo, and D. A. Scherlis, J. Phys. Chem. C **112**, 17611 (2008).
[31] Y. Imry and R. Landauer, Rev. Mod. Phys. **71**, S306 (1999).
[32] D. Kalkstein and P. Soven, Surf. Sci. **26**, 85 (1971).
[33] T. L. Einstein and J. R. Schrieffer, Phys. Rev. B **7**, 3629 (1973).
[34] M. G. Reuter, J. Chem. Phys. **133**, 034703 (2010).
[35] N. R. Burke, Surf. Sci. **58**, 349 (1976).
[36] R. Hoffmann, Rev. Mod. Phys. **60**, 601 (1988).
[37] S. Datta, *Electronic Transport in Mesoscopic Systems* (Cambridge University Press, Cambridge, England, 1995).
[38] $\Sigma(E)$ is formally an operator; however, since the molecular wire has only one state ($|\varphi\rangle$), we often consider $\Sigma(E)$ to be the scalar $\langle\varphi|\Sigma(E)|\varphi\rangle$. The six $\Sigma(E)$ listed in Table II and Eq. (6), as written, are already the scalar values.
[39] We neglect molecular level shifting by setting $\mathrm{Re}\Sigma(E) = 0$.

Downloaded 29 Jul 2011 to 129.105.55.246. Redistribution subject to AIP license or copyright; see http://jcp.aip.org/about/rights_and_permissions